metals

MDPI

Article

Generation Mechanism of MgO and Al_2O_3 Inclusions in 51CrV4 Spring Steel Based on the Ion–Molecule Coexistence Theory

Jialiu Lei [1,*], Hangyu Zhu [2], Dongnan Zhao [1] and Zhengliang Xue [2]

[1] School of Materials Science and Engineering, Hubei Polytechnic University, Huangshi 435000, China
[2] The State Key Laboratory of Refractories and Metallurgy, Wuhan University of Science and Technology, Wuhan 430081, China
* Correspondence: leijialiu@hbpu.edu.cn; Tel.: +86-0714-635-8328

Received: 1 July 2019; Accepted: 24 July 2019; Published: 26 July 2019

Abstract: The presence of $MgO{\cdot}Al_2O_3$ inclusions in 51CrV4 spring steel is detrimental to the alloy's castability and fatigue properties. To effectively suppress these inclusions during production, accretions were collected from the immersion nozzle, and the $MgO{\cdot}Al_2O_3$ inclusions in the steel billet were investigated. The generation mechanism of the inclusions was evaluated based on the ion–molecule coexistence theory, and the mass action–concentration model of $CaO–SiO_2–Al_2O_3–MgO–FeO–MnO$ slag was developed. Industrial experiments showed that nozzle clogging was primarily caused by $MgAl_2O_4$ spinel inclusions, and the $MgO{\cdot}Al_2O_3$ spinel inclusions in the steel billet were investigated by non-aqueous electrolysis. The model calculation results indicate that the Mg content increased with an increasing basicity, CaO/Al_2O_3 ratio, and Al content during the ladle furnace (LF) process. In contrast, the Mg content decreased with increasing CO pressure under Ruhstahl-Hausen vacuum degassing process (RH) conditions.

Keywords: $MgO{\cdot}Al_2O_3$ inclusions; mass action–concentration model; slag basicity; CaO/Al_2O_3 ratio; ion–molecule coexistence theory

1. Introduction

In recent years, the increasing demand for alloyed steels with excellent properties has led to efforts to enhance the castability, surface quality, toughness, and fatigue behaviors of alloyed steels [1–4]. Due to the addition of Cr and V, 51CrV4 spring steel exhibits an excellent intensity, fatigue performance, and hardenability; thus, it has attracted considerable attention for use in large damping springs, suspension springs, and flat springs [5,6]. During the production of 51CrV4 steel, a high-basicity slag is adopted, as it is conductive to the removal of inclusions in bulk steel, desulfurization, and reducing the total oxygen content, but results in the formation of detrimental $MgO{\cdot}Al_2O_3$ inclusions [7–9]. These inclusions have a steady face-centered cubic structure with a high melting point and are hard and un-deformable [10]. They tend to accumulate on the submerged entry nozzle (SEN) [2,11,12], resulting in nozzle clogging during casting. Furthermore, the accretions on the SEN might desquamate and become entrapped in the solidified shell, resulting in serious decreases in the internal quality [13]. Therefore, $MgO{\cdot}Al_2O_3$ inclusions are detrimental to the final 51CrV4 product and its castability. Although a small amount of dissolved Ca can modify the $MgO{\cdot}Al_2O_3$ spinel inclusions [9,14–17], the Ca treatment has a limited effect on large clusters of $MgO{\cdot}Al_2O_3$ inclusions [18].

The generation and control of $MgO{\cdot}Al_2O_3$ inclusions in stainless steels have been extensively investigated, because these inclusions are harmful to both the surface quality and forming properties of the final products [2,8,19–22]. They are thought to be generated from sources of Mg in liquid steel

via the reduction of MgO in slag or MgO-based refractory [8,23–25]. Many studies have found that the compositions of top slag and refractory material strongly affect the inclusion composition [16,17,21,26–37], as summarized in Table 1.

Table 1. The relationships between compositions of slag or refractory and inclusions.

Steels	Slag/Refractory	Inclusions	Main Finding	Ref.
High strength alloyed structural steel	CaO–SiO_2–Al_2O_3–MgO	MgO·Al_2O_3	log($XMgO/XAl_2O_3$) of inclusions and log($aMgO/aAl_2O_3$) in slag exhibiting a good linear relation.	[16]
High strength alloying steel	CaO–SiO_2–Al_2O_3	MgO·Al_2O_3–CaO	MgO·Al_2O_3 inclusions can be modified to liquid ones by high-basicity slag.	[17]
Ferritic stainless steel	CaO–Al_2O_3–MgO	MgO·Al_2O_3	log($XMgO/XAl_2O_3$) of inclusions and log($aMgO/aAl_2O_3$) in slag showing a good linear relation.	[21]
Al-killed ferritic stainless steel	CaO–SiO_2–Al_2O_3–MgO	MgO·Al_2O_3	MgO contents in inclusions decreased with the declining of CaO/SiO_2 and CaO/Al_2O_3 ratio.	[26]
Mn and V alloyed steel	CaO–SiO_2–Al_2O_3–MgO–CaF_2	Spinel	The generation behavior of inclusion was influenced by *a*MgO in the initial slag.	[27]
Al-killed steel	CaO–SiO_2–Al_2O_3–MgO–FeO	MgO·Al_2O_3	The content of FeO in slag plays an important role in the formation of MgO·Al_2O_3 inclusions.	[28]
Bearing steel	CaO–SiO_2–Al_2O_3–MgO	CaO–SiO_2–Al_2O_3–MgO	Thermodynamic for the formation of spinel inclusions was made.	[29]
Fe–Mn–S–C–Al steel	CaO–Al_2O_3–SiO_2–CaF_2–MgO/MgO–C refractory	$MgAl_2O_4$	The calculated results at different composition of slag and steel were in good agreement with the experimental results.	[30]
Extra-low-oxygen steel	MgO-based refractory and MgO bearing slag	MgO·Al_2O_3 spinel	MgO-based refractory supplied more Mg into liquid steel than refining slag.	[31]
Al deoxidized molten steel	MgO–C refractory	MgO·Al_2O_3	An internal oxidation-reduction occurs in the MgO–C refractory at elevated temperature.	[32]
Al-killed molten steel	Mg–Cr refractory	MgO·Al_2O_3 spinel	Mg and Cr dissolved from the refractory, and lead to the increasing contents of Mg and Cr in the liquid steel.	[33]
Fe–Al alloy	MgO-based refractory	MgO·Al_2O_3 spinel	The generation of a spinel layer at the interface was attributing to oxidation–reduction reactions and phase transformation.	[34]
Steels	MgO-based refractory	Spinel	Improving the resistance of MgO-based refractory to slag penetration is good to improve steel cleanness.	[35]
Al-killed steel	MgO refractory	Spinel	The decomposing of MgO refractory plays a key role in the dissolution of MgO refractory in Al-killed steels.	[36]
304 stainless steel	CaO–Al_2O_3-based slag	Spinel	A thermodynamic model was developed to predict slag–steel–inclusion reactions.	[37]

Compared to stainless steels, the suppression of MgO·Al_2O_3 inclusions in alloyed spring steels has the potential to provide a superior castability and fatigue performance. In this study, the generation mechanism of MgO·Al_2O_3 inclusions in 51CrV4 spring steel refined by CaO–SiO_2–Al_2O_3–MgO–FeO–MnO slag was investigated, based on the ion–molecule coexistence theory (IMCT) combined with industrial experiments, and influential factors were discussed.

2. Experimental and Methods

2.1. Nozzle Clogging

Nozzle clogging is occasionally observed during the production of 51Cr4V steel. To understand the causes of nozzle clogging, accretions taken from the SEN were identified by X-ray diffraction (XRD) and scanning electron microscopy (SEM) equipped with energy-dispersive X-ray spectroscopy (EDS). The XRD analysis indicated that the accretions primarily consisted of $MgAl_2O_4$ (Figure 1).

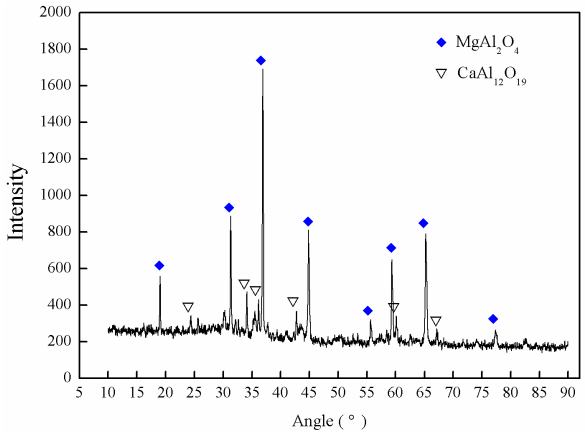

Figure 1. X-ray diffraction (XRD) pattern of the accretion collected from the submerged entry nozzle (SEN).

An image of the collected accretion is shown in Figure 2. The XRD and EDS analyses indicated that the accretion was composed of $MgO{\cdot}Al_2O_3$ spinel (dark phase) and $CaO{\cdot}6Al_2O_3$ hexa-aluminate (gray phase). Therefore, the XRD and SEM/EDS analyses indicated that nozzle clogging was primarily caused by the presence of $MgAl_2O_4$ spinel inclusions. Moreover, if the accretions desquamated from the nozzle wall, they would be entrapped by the solidified shell and lead to a decreased quality.

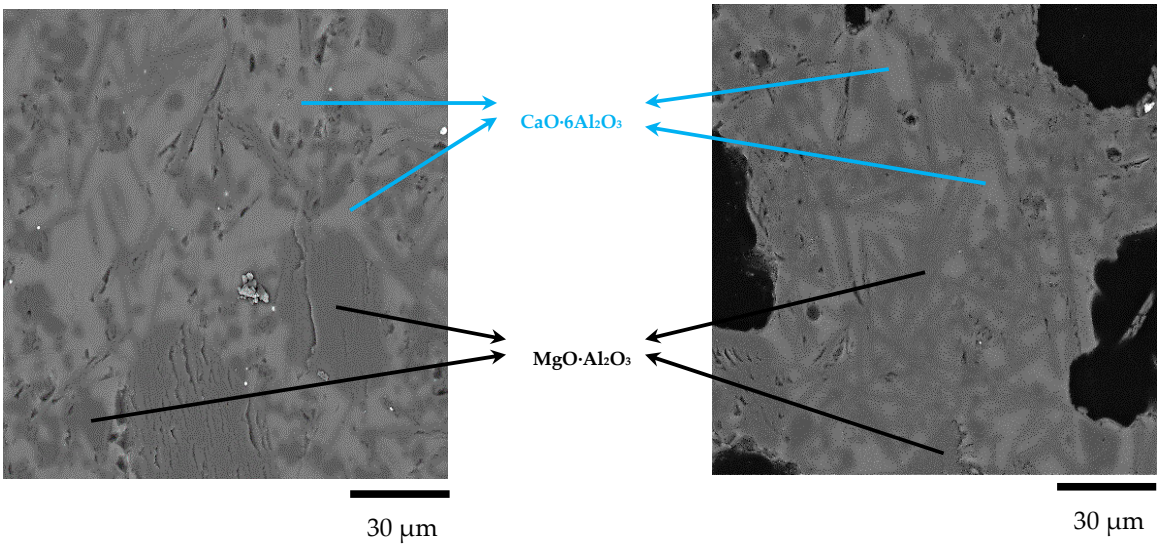

Figure 2. Scanning electron microscopy (SEM) images of the accretion.

2.2. Types of $MgO{\cdot}Al_2O_3$ Spinel Inclusions in 51CrV4 Spring Steel

The smelting process of 51CrV4 spring steel can be described as BOF→LF→RH→calcium treatment (soft blow)→slab continuous casting. During basic oxygen furnace (BOF) tapping, Al ingots were employed for preliminary deoxidation and V–Fe and Cr–Fe as the alloying elements. When the ladle reached the ladle furnace (LF) station, a high-basicity slag was used, and Al particles were added into liquid steel for final deoxidation. During the LF process, V–Fe and Cr–Fe were added to final composition adjustment. After degassing in Ruhstahl-Hausen vacuum degassing process (RH) for 20 min, the Ca–Si wire was fed to modify the inclusions and the removal of inclusions by soft blowing about 15 min was done. Finally, the liquid steel was sent to the continuous casting (CC) platform. The average compositions of 51CrV4 spring steel and refining slag are given in Tables 2 and 3, respectively.

Table 2. Average composition of 51CrV4 spring steel (wt%).

C	Si	Mn	P	S	Al	Cr	V	Fe
0.51	0.23	0.94	0.01	0.008	0.024	1.02	0.16	balance

Table 3. Average composition of refining slag (wt%).

CaO	SiO_2	MgO	FeO	MnO	Al_2O_3	CaO/Al_2O_3
50.19	8.2	7.49	0.35	0.18	33.59	1.49

Three types of $MgO{\cdot}Al_2O_3$ spinel inclusions in the steel billet were evaluated via non-aqueous electrolysis: Independent $MgO{\cdot}Al_2O_3$ inclusions (Figure 3a); modified $MgO{\cdot}Al_2O_3$ spinel inclusions primarily containing Mg, Ca, Al, and O (Figure 3b), which was the dominant inclusion type; and modified spinel inclusions mainly consisting of Al, Ca, and O (Figure 3c). The spinel-type inclusions exhibited three-dimensional shapes with spherical morphologies, and the energy spectra given in Figure 3 are all for point A.

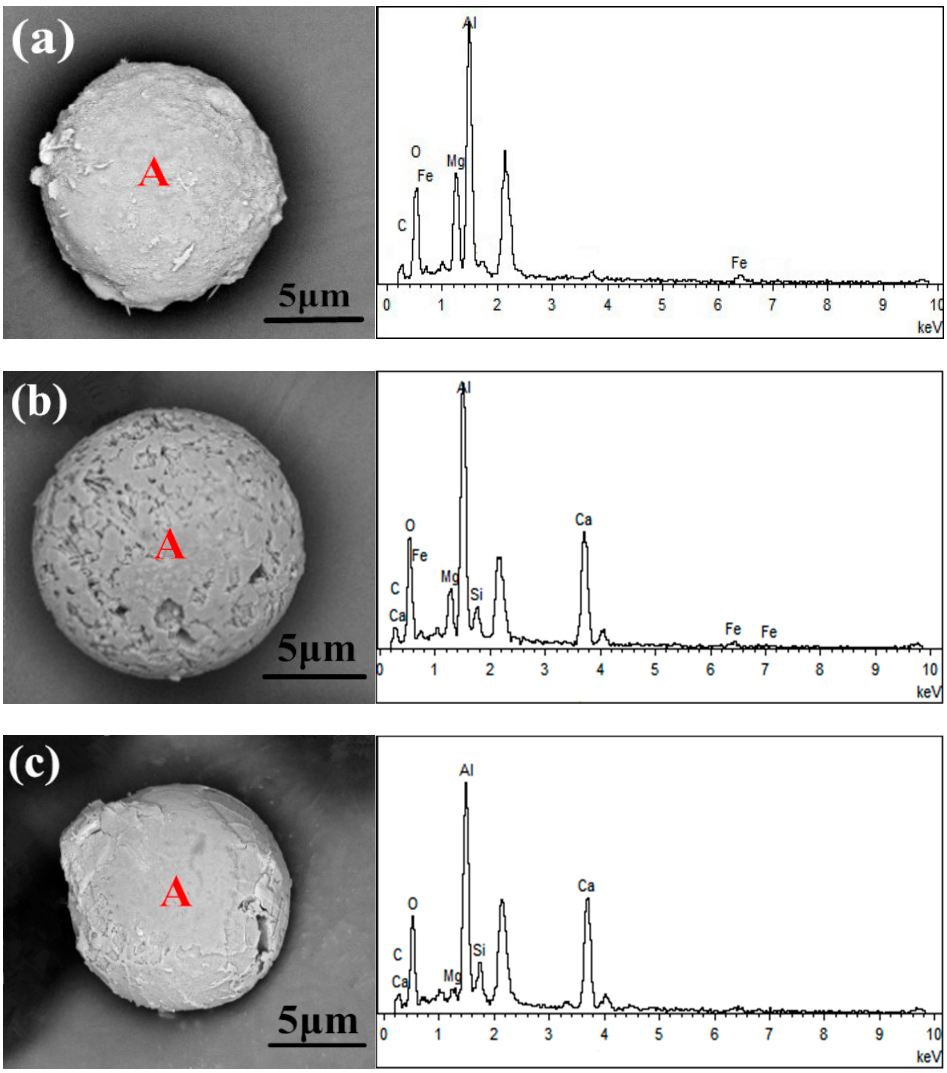

Figure 3. Images and energy spectra of $MgO{\cdot}Al_2O_3$ spinel-type inclusions extracted by non-aqueous electrolysis: (**a**) Independent $MgO{\cdot}Al_2O_3$ inclusions; (**b**) modified spinel inclusions containing Mg, Ca, Al, and O; (**c**) modified spinel inclusions consisting of Al, Ca, and O.

To assess the inclusions during the LF refining process, RH, and calcium treatment, respectively, the steel specimens taken with pail samplers were also investigated before and after LF and RH after polishing; the schematic diagram of sampling locations is given in Figure 4.

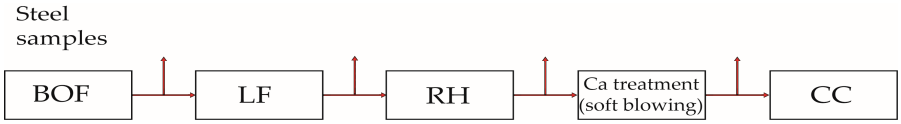

Figure 4. Schematic diagram of sampling locations.

The evolution of mean mass fraction of inclusions in the specimens is shown in Figure 5. Figure 5 indicated that no $MgO{\cdot}Al_2O_3$ spinel inclusions were found before LF; $MgO{\cdot}Al_2O_3$ inclusions containing small amounts of CaO began to form after LF. The number of $MgO{\cdot}Al_2O_3$ spinel inclusions increased after RH, and the dominant inclusion type was $MgO–Al_2O_3–CaO$, which was attributed to the calcium treatment after RH. Therefore, the inclusions transformed through $Al_2O_3 \rightarrow MgO{\cdot}Al_2O_3 \rightarrow MgO–Al_2O_3–CaO$ during the refining process.

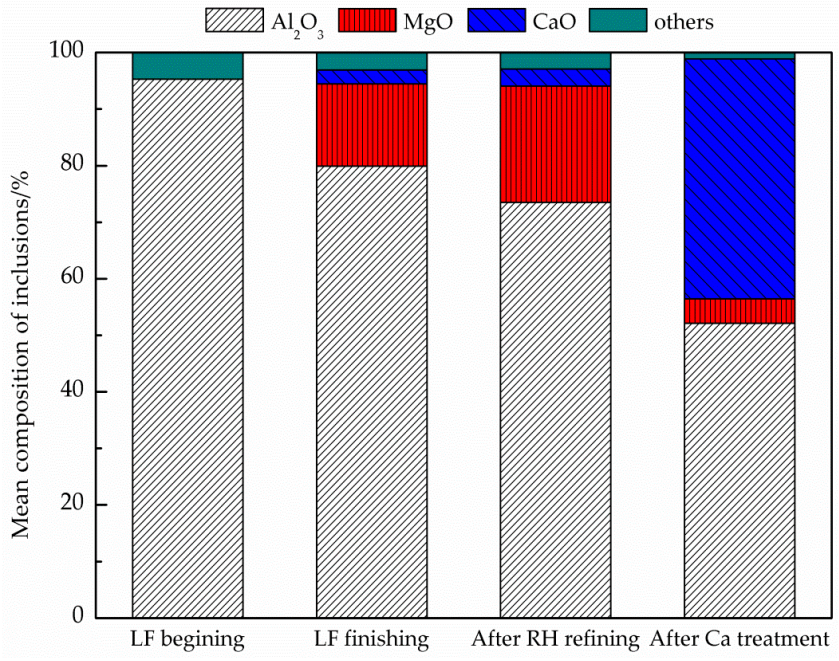

Figure 5. Evolution of mean mass fraction of inclusions.

2.3. Generation Mechanism of $MgO{\cdot}Al_2O_3$ Inclusions

There are four possible Mg sources in liquid steel (Figure 6) [8,13,25,26,38–40]: (1) The reduction of MgO in slag by Al in liquid steel; (2) the reduction of MgO in slag by C under RH conditions; (3) the reduction of MgO in the refractory by Al in liquid steel; and (4) the reduction of MgO in the refractory by C under RH conditions.

The reduced Mg in liquid steel is oxidized into MgO and reacts with Al_2O_3 to generate $MgO{\cdot}Al_2O_3$ inclusions via the following reactions:

$$2[Al] + 3(MgO) = (Al_2O_3) + 3[Mg], \quad (1)$$

$$[C] + (MgO) = [Mg] + CO_{(g)}, \quad (2)$$

$$[Mg] + [O] = (MgO), \quad (3)$$

and

$$(MgO) + (Al_2O_3) = (MgO{\cdot}Al_2O_3). \quad (4)$$

Therefore, to suppress the formation of $MgAl_2O_4$ inclusions during steel production, it is essential to study the generation mechanism of inclusions along with the factors influencing their formation. However, it is difficult to determine the activity of each constituent in a complex refining slag. The IMCT provides an effective way to obtain the activity of a complicated slag [41–56]. In the IMCT, the defined mass action–concentration (MAC) is consistent with the classical concept of activity in the slag. The MAC model based on the IMCT has been successfully applied to describe the manganese distribution, phosphate capacity, sulfide capacity, and so on [41–56].

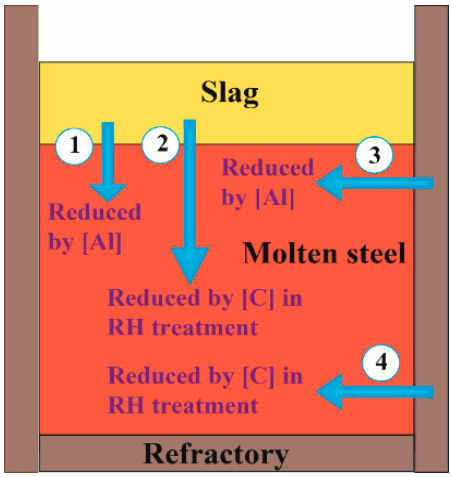

Figure 6. Diagram showing the four potential sources of Mg in liquid steel.

2.4. MAC Model of the Constitutional Units in Slag Systems

Based on the assumptions inherent in the IMCT, the dominant features of the MAC model for the activities of the structural units in the slag can be summarized as follows:

(1) The constitutional units in the slag consist of simple ions, ordinary molecules, and complicated molecules;

(2) Complex molecules are generated by the reactions of bonded ion couples and simple molecules under kinetic equilibrium;

(3) The activity of each constituent in the slag equals the MAC of the structural unit at the steelmaking temperature;

(4) The chemical reactions comply with the law of mass conservation.

The calculations were based on actual production involving $CaO–SiO_2–Al_2O_3–MgO–FeO–MnO$ slag systems. The initial numbers of moles for each composition in 100g of $CaO–SiO_2–Al_2O_3–MgO–FeO–MnO$ slag were $a = n^0_{CaO}$, $b = n^0_{SiO_2}$, $c = n^0_{Al_2O_3}$, $d = n^0_{MgO}$, $e = n^0_{FeO}$, and $f = n^0_{MnO}$, respectively. The balanced mole number of each constituent unit in the slag was defined as n_i, and N_i denotes the MAC of each constitutional unit. The MAC is equivalent to the classical definition of activity based on the IMCT and can be obtained as follows:

$$N_i = \frac{n_i}{\sum n_i} \quad (5)$$

where $\sum n_i$ is the total balanced mole number of each constitutional unit.

According to the IMCT, at an elevated temperature, the slag system contains four simple ions (Ca^{2+}, Mg^{2+}, Fe^{2+}, Mn^{2+}, and O^{2-}) and two ordinary molecules (Al_2O_3 and SiO_2). Based on the reported phase diagrams, 25 types of complex molecules can be generated at the steelmaking temperature [57,58]. The above mentioned structural units and their parameters are listed in Table 4.

Table 4. Parameters of the structural units in the slag system.

Items	Constitutional Units	Balanced Mole Number	Mass Action–Concentrations (MACs)
Simple cations and anions	$Ca^{2+} + O^{2-}$	$n_1 = n_{Ca^{2+}} = n_{O^{2-}} = n_{CaO}$	$N_1 = \frac{2n_1}{\sum n_i} = N_{CaO}$
	$Mg^{2+} + O^{2-}$	$n_4 = n_{Mg^{2+}} = n_{O^{2-}} = n_{MgO}$	$N_4 = \frac{2n_4}{\sum n_i} = N_{MgO}$
	$Fe^{2+} + O^{2-}$	$n_5 = n_{Fe^{2+}} = n_{O^{2-}} = n_{FeO}$	$N_5 = \frac{2n_5}{\sum n_i} = N_{FeO}$
	$Mn^{2+} + O^{2-}$	$n_6 = n_{Mn^{2+}} = n_{O^{2-}} = n_{MnO}$	$N_6 = \frac{2n_6}{\sum n_i} = N_{MnO}$
Simple molecules	SiO_2	$n_2 = n_{SiO_2}$	$N_2 = \frac{n_2}{\sum n_i} = N_{SiO_2}$
	Al_2O_3	$n_3 = n_{Al_2O_3}$	$N_3 = \frac{n_3}{\sum n_i} = N_{Al_2O_3}$
Complex molecules	$CaO{\cdot}SiO_2$	$n_7 = n_{CaO{\cdot}SiO_2}$	$N_7 = \frac{n_7}{\sum n_i} = N_{CaO{\cdot}SiO_2}$
	$3CaO{\cdot}2SiO_2$	$n_8 = n_{3CaO{\cdot}2SiO_2}$	$N_8 = \frac{n_8}{\sum n_i} = N_{3CaO{\cdot}2SiO_2}$
	$2CaO{\cdot}SiO_2$	$n_9 = n_{2CaO{\cdot}SiO_2}$	$N_9 = \frac{n_9}{\sum n_i} = N_{2CaO{\cdot}SiO_2}$
	$3CaO{\cdot}SiO_2$	$n_{10} = n_{3CaO{\cdot}SiO_2}$	$N_{10} = \frac{n_{10}}{\sum n_i} = N_{3CaO{\cdot}SiO_2}$
	$3CaO{\cdot}Al_2O_3$	$n_{11} = n_{3CaO{\cdot}Al_2O_3}$	$N_{11} = \frac{n_{11}}{\sum n_i} = N_{3CaO{\cdot}Al_2O_3}$
	$12CaO{\cdot}7Al_2O_3$	$n_{12} = n_{12CaO{\cdot}7Al_2O_3}$	$N_{12} = \frac{n_{12}}{\sum n_i} = N_{12CaO{\cdot}7Al_2O_3}$
	$CaO{\cdot}Al_2O_3$	$n_{13} = n_{CaO{\cdot}Al_2O_3}$	$N_{13} = \frac{n_{13}}{\sum n_i} = N_{CaO{\cdot}Al_2O_3}$
	$CaO{\cdot}2Al_2O_3$	$n_{14} = n_{CaO{\cdot}2Al_2O_3}$	$N_{14} = \frac{n_{14}}{\sum n_i} = N_{CaO{\cdot}2Al_2O_3}$
	$CaO{\cdot}6Al_2O_3$	$n_{15} = n_{CaO{\cdot}6Al_2O_3}$	$N_{15} = \frac{n_{15}}{\sum n_i} = N_{CaO{\cdot}6Al_2O_3}$
	$3Al_2O_3{\cdot}2SiO_2$	$n_{16} = n_{3Al_2O_3{\cdot}2SiO_2}$	$N_{16} = \frac{n_{16}}{\sum n_i} = N_{3Al_2O_3{\cdot}2SiO_2}$
	$2MgO{\cdot}SiO_2$	$n_{17} = n_{2MgO{\cdot}SiO_2}$	$N_{17} = \frac{n_{17}}{\sum n_i} = N_{2MgO{\cdot}SiO_2}$
	$MgO{\cdot}SiO_2$	$n_{18} = n_{MgO{\cdot}SiO_2}$	$N_{18} = \frac{n_{18}}{\sum n_i} = N_{MgO{\cdot}SiO_2}$
	$MgO{\cdot}Al_2O_3$	$n_{19} = n_{MgO{\cdot}Al_2O_3}$	$N_{19} = \frac{n_{19}}{\sum n_i} = N_{MgO{\cdot}Al_2O_3}$
	$2FeO{\cdot}SiO_2$	$n_{20} = n_{2FeO{\cdot}SiO_2}$	$N_{20} = \frac{n_{20}}{\sum n_i} = N_{2FeO{\cdot}SiO_2}$
	$FeO{\cdot}Al_2O_3$	$n_{21} = n_{FeO{\cdot}Al_2O_3}$	$N_{21} = \frac{n_{21}}{\sum n_i} = N_{FeO{\cdot}Al_2O_3}$
	$MnO{\cdot}SiO_2$	$n_{22} = n_{MnO{\cdot}SiO_2}$	$N_{22} = \frac{n_{22}}{\sum n_i} = N_{MnO{\cdot}SiO_2}$
	$2MnO{\cdot}SiO_2$	$n_{23} = n_{2MnO{\cdot}SiO_2}$	$N_{23} = \frac{n_{23}}{\sum n_i} = N_{2MnO{\cdot}SiO_2}$
	$MnO{\cdot}Al_2O_3$	$n_{24} = n_{MnO{\cdot}Al_2O_3}$	$N_{24} = \frac{n_{24}}{\sum n_i} = N_{MnO{\cdot}Al_2O_3}$
	$2CaO{\cdot}Al_2O_3{\cdot}SiO_2$	$n_{25} = n_{2CaO{\cdot}Al_2O_3{\cdot}SiO_2}$	$N_{25} = \frac{n_{25}}{\sum n_i} = N_{2CaO{\cdot}Al_2O_3{\cdot}SiO_2}$
	$CaO{\cdot}Al_2O_3{\cdot}2SiO_2$	$n_{26} = n_{CaO{\cdot}Al_2O_3{\cdot}2SiO_2}$	$N_{26} = \frac{n_{26}}{\sum n_i} = N_{CaO{\cdot}Al_2O_3{\cdot}2SiO_2}$
	$2CaO{\cdot}MgO{\cdot}2SiO_2$	$n_{27} = n_{2CaO{\cdot}MgO{\cdot}2SiO_2}$	$N_{27} = \frac{n_{27}}{\sum n_i} = N_{2CaO{\cdot}MgO{\cdot}2SiO_2}$
	$3CaO{\cdot}MgO{\cdot}2SiO_2$	$n_{28} = n_{3CaO{\cdot}MgO{\cdot}2SiO_2}$	$N_{28} = \frac{n_{28}}{\sum n_i} = N_{3CaO{\cdot}MgO{\cdot}2SiO_2}$
	$CaO{\cdot}MgO{\cdot}SiO_2$	$n_{29} = n_{CaO{\cdot}MgO{\cdot}SiO_2}$	$N_{29} = \frac{n_{29}}{\sum n_i} = N_{CaO{\cdot}MgO{\cdot}SiO_2}$
	$CaO{\cdot}MgO{\cdot}2SiO_2$	$n_{30} = n_{CaO{\cdot}MgO{\cdot}2SiO_2}$	$N_{30} = \frac{n_{30}}{\sum n_i} = N_{CaO{\cdot}MgO{\cdot}2SiO_2}$
	$2MgO{\cdot}2Al_2O_3{\cdot}5SiO_2$	$n_{31} = n_{2MgO{\cdot}2Al_2O_3{\cdot}5SiO_2}$	$N_{31} = \frac{n_{31}}{\sum n_i} = N_{2MgO{\cdot}2Al_2O_3{\cdot}5SiO_2}$

The MACs for all the complex molecules can be determined using the reaction equilibrium constants K_i, $N_1(N_{CaO})$, $N_2(N_{SiO_2})$, $N_3(N_{Al_2O_3})$, $N_4(N_{MgO})$, $N_5(N_{FeO})$, and $N_6(N_{MnO})$, which are listed in Table 5.

The mass conservation equations for the CaO–SiO_2–Al_2O_3–MgO–FeO–MnO slag equilibrated with bulk steel can be built based on the definitions of n_i and N_i for each structural unit as follows:

$$a = \sum n_i(0.5N_1 + N_7 + 3N_8 + 2N_9 + 3N_{10} + 3N_{11} + 12N_{12} + N_{13} + N_{14} + N_{15} + 2N_{25} + N_{26} + 2N_{27} + 3N_{28} + N_{29} + N_{30}) \quad (6)$$

$$b = \sum n_i(N_2 + N_7 + 2N_8 + N_9 + N_{10} + 2N_{16} + N_{17} + N_{18} + N_{20} + N_{22} + N_{23} + N_{25} + 2N_{26} + 2N_{27} + 2N_{28} + N_{29} + 2N_{30} + 5N_{31}) \quad (7)$$

$$c = \sum n_i(N_3 + N_{11} + 7N_{12} + N_{13} + 2N_{14} + 6N_{15} + 3N_{16} + N_{19} + N_{21} + N_{24} + N_{25} + N_{26} + 2N_{31}) \quad (8)$$

$$d = \sum n_i(0.5N_4 + 2N_{17} + N_{18} + N_{19} + N_{27} + N_{28} + N_{29} + N_{30} + 2N_{31}) \quad (9)$$

$$e = \sum n_i(0.5N_5 + 2N_{20} + N_{21}) \quad (10)$$

and

$$f = \sum n_i(0.5N_6 + N_{22} + 2N_{23} + N_{24}). \quad (11)$$

Based on the theory that the total MAC of each constitutional unit in CaO–SiO_2–Al_2O_3–MgO–FeO–MnO slag with a fixed amount is equal to unity, Equation (12) can be derived as follows:

$$\sum_{i=1}^{31} N_i = 1. \quad (12)$$

Equations (5)–(12) represent the MAC calculation model for each constitutional unit in CaO–SiO_2–Al_2O_3–MgO–FeO–MnO slag systems. The activity of each constituent in the slag at the refining temperature can then be obtained.

Table 5. Reaction formulas, Gibbs free energies, and mass action–concentrations (MACs) [56,59–64].

Reaction Formulas	$\Delta G^\theta/(\mathrm{J\cdot mol^{-1}})$	MACs
$(Ca^{2+} + O^{2-}) + (SiO_2) = (CaO{\cdot}SiO_2)$	$\Delta G^\theta = -21757 - 36.819T$	$N_7 = K_1N_1N_2$
$3(Ca^{2+} + O^{2-}) + 2(SiO_2) = (3CaO{\cdot}2SiO_2)$	$\Delta G^\theta = -236972.9 + 9.6296T$	$N_8 = K_2N_1^3N_2^2$
$2(Ca^{2+} + O^{2-}) + (SiO_2) = (2CaO{\cdot}SiO_2)$	$\Delta G^\theta = -102090 - 24.267T$	$N_9 = K_3N_1^2N_2$
$3(Ca^{2+} + O^{2-}) + (SiO_2) = (3CaO{\cdot}SiO_2)$	$\Delta G^\theta = -118826 - 6.694T$	$N_{10} = K_4N_1^3N_2$
$3(Ca^{2+} + O^{2-}) + (Al_2O_3) = (3CaO{\cdot}Al_2O_3)$	$\Delta G^\theta = -21757 - 29.288T$	$N_{11} = K_5N_1^3N_3$
$12(Ca^{2+} + O^{2-}) + 7(Al_2O_3) = (12CaO{\cdot}7Al_2O_3)$	$\Delta G^\theta = 617977 - 612.119T$	$N_{12} = K_6N_1^{12}N_3^7$
$(Ca^{2+} + O^{2-}) + (Al_2O_3) = (CaO{\cdot}Al_2O_3)$	$\Delta G^\theta = 59413 - 59.413T$	$N_{13} = K_7N_1N_3$
$(Ca^{2+} + O^{2-}) + 2(Al_2O_3) = (CaO{\cdot}2Al_2O_3)$	$\Delta G^\theta = -16736 - 25.522T$	$N_{14} = K_8N_1N_3^2$
$(Ca^{2+} + O^{2-}) + 6(Al_2O_3) = (CaO{\cdot}6Al_2O_3)$	$\Delta G^\theta = -22594 - 31.798T$	$N_{15} = K_9N_1N_3^6$
$3(Al_2O_3) + 2(SiO_2) = (3Al_2O_3{\cdot}2SiO_2)$	$\Delta G^\theta = -4351 - 10.46T$	$N_{16} = K_{10}N_2^2N_3^3$
$2(Mg^{2+} + O^{2-}) + (SiO_2) = (2MgO{\cdot}SiO_2)$	$\Delta G^\theta = -56902 - 3.347T$	$N_{17} = K_{11}N_2N_4^2$
$(Mg^{2+} + O^{2-}) + (SiO_2) = (MgO{\cdot}SiO_2)$	$\Delta G^\theta = 23849 - 29.706T$	$N_{18} = K_{12}N_2N_4$
$(Mg^{2+} + O^{2-}) + (Al_2O_3) = (MgO{\cdot}Al_2O_3)$	$\Delta G^\theta = -18828 - 6.276T$	$N_{19} = K_{13}N_3N_4$
$2(Fe^{2+} + O^{2-}) + (SiO_2) = (2FeO{\cdot}SiO_2)$	$\Delta G^\theta = -9395 - 0.227T$	$N_{20} = K_{14}N_2N_5^2$
$(Fe^{2+} + O^{2-}) + (Al_2O_3) = (FeO{\cdot}Al_2O_3)$	$\Delta G^\theta = -59204 + 22.343T$	$N_{21} = K_{15}N_3N_5$
$(Mn^{2+} + O^{2-}) + (SiO_2) = (MnO{\cdot}SiO_2)$	$\Delta G^\theta = 38911 - 40.041T$	$N_{22} = K_{16}N_2N_6$
$2(Mn^{2+} + O^{2-}) + (SiO_2) = (2MnO{\cdot}SiO_2)$	$\Delta G^\theta = 36066 - 30.669T$	$N_{23} = K_{17}N_2N_6^2$
$(Mn^{2+} + O^{2-}) + (Al_2O_3) = (MnO{\cdot}Al_2O_3)$	$\Delta G^\theta = -45116 + 11.81T$	$N_{24} = K_{18}N_3N_6$
$2(Ca^{2+} + O^{2-}) + (Al_2O_3) + (SiO_2) = (2CaO{\cdot}Al_2O_3{\cdot}SiO_2)$	$\Delta G^\theta = -116315 - 38.911T$	$N_{25} = K_{19}N_1^2N_2N_3$
$(Ca^{2+} + O^{2-}) + (Al_2O_3) + 2(SiO_2) = (CaO{\cdot}Al_2O_3{\cdot}2SiO_2)$	$\Delta G^\theta = -4148 - 73.638T$	$N_{26} = K_{20}N_1N_2^2N_3$
$2(Ca^{2+} + O^{2-}) + (Mg^{2+} + O^{2-}) + 2(SiO_2) = (2CaO{\cdot}MgO{\cdot}2SiO_2)$	$\Delta G^\theta = -73638 - 63.597T$	$N_{27} = K_{21}N_1^2N_2^2N_4$
$3(Ca^{2+} + O^{2-}) + (Mg^{2+} + O^{2-}) + 2(SiO_2) = (3CaO{\cdot}MgO{\cdot}2SiO_2)$	$\Delta G^\theta = -205016 - 31.798T$	$N_{28} = K_{22}N_1^3N_2^2N_4$
$(Ca^{2+} + O^{2-}) + (Mg^{2+} + O^{2-}) + (SiO_2) = (CaO{\cdot}MgO{\cdot}SiO_2)$	$\Delta G^\theta = -124683 + 3.766T$	$N_{29} = K_{23}N_1N_2N_4$
$(Ca^{2+} + O^{2-}) + (Mg^{2+} + O^{2-}) + 2(SiO_2) = (CaO{\cdot}MgO{\cdot}2SiO_2)$	$\Delta G^\theta = -80333 - 51.882T$	$N_{30} = K_{24}N_1N_2^2N_4$
$2(Mg^{2+} + O^{2-}) + 2(Al_2O_3) + 5(SiO_2) = (2MgO{\cdot}2Al_2O_3{\cdot}5SiO_2)$	$\Delta G^\theta = -14422 - 14.808T$	$N_{31} = K_{25}N_2^5N_3^2N_4^2$

3. Results and Discussions

3.1. Effect of Slag Composition on Mg Content in Liquid Steel

After final deoxidation with Al, the dissolved Mg is supplied by the reduction of MgO in slag by dissolved Al via the following reaction [65]:

$$2[\mathrm{Al}] + 3(\mathrm{MgO})_s = (Al_2O_3)_s + 3[\mathrm{Mg}],\ \Delta G^0 = 296752.4 + 21.69T(\frac{\mathrm{J}}{\mathrm{mol}}). \quad (13)$$

The equilibrium constant K for the above process is given by

$$K = \frac{(a_{Al_2O_3,slag} \cdot a_{Mg}^3)}{(a_{MgO,slag}^3 \cdot a_{Al}^2)} = \frac{(a_{Al_2O_3,slag} \cdot f_{Mg}^3 \cdot [\%Mg]^3)}{(a_{MgO,slag}^3 \cdot f_{Al}^2 \cdot [\%Al]^2)} = \exp\left(\frac{-\Delta G^0}{RT}\right) \quad (14)$$

where $a_{MgO,slag}$ and $a_{Al_2O_3,slag}$ are the activities of MgO and Al_2O_3 in slag relative to the pure solid state, respectively; a_{Mg} and a_{Al} are the activities of Mg and Al in liquid steel relative to a 1% mass concentration, respectively; and f_{Mg} and f_{Al} are the activity coefficients of Mg and Al in molten steel, respectively. R is the ideal gas constant, whose value is 8.314 J/(mol·K).

The interaction coefficients e_i^j are given in Table 6. The relationship between the activity coefficient f_i and temperature can be described as follows [66]:

$$\lg f_i(T) = \left(\frac{2538}{T} - 0.355\right) \lg f_i(1873\ K) \quad (15)$$

where

$$\lg f_i(1873\ K) = \sum e_i^j [\%j]. \quad (16)$$

Table 6. Interaction coefficients for bulk steel at 1873 K [29,58].

e_i^j	C	Si	Mn	P	S	Al	Cr	V
C	0.14	0.08	−0.012	0.051	0.046	0.043	−0.024	−0.077
Mg	−0.24	−0.09	–	–	−1.38	−0.12	0.05	–
Al	0.091	0.0056	0.0065	0.033	0.030	0.045	0.012	0.06

By substituting the values of f_{Mg} and f_{Al} at 1853 K (0.781 and 1.198, respectively) into Equation (14), the effect of the slag composition on the content of Mg at 1853 K is obtained as follows:

$$[\%Mg] = 1.44 \times 10^{-3.17} N_{MgO} \left(\frac{[\%Al]^2}{N_{Al_2O_3}}\right)^{\frac{1}{3}}. \quad (17)$$

Based on the constituents of refining slag shown in Table 3, the compositions of MgO, FeO, and MnO were fixed at 7.5 wt%, 0.35 wt%, and 0.2 wt%, respectively, in subsequent calculations.

Equation (17) gives the thermodynamic model of MgO in slag reduced by Al. Based on the MAC model, N_{MgO} and N_{Al2O3} at various basicities and CaO/Al_2O_3 ratios were calculated, and the relationship between Al and Mg content was obtained (Figure 7). The content of Mg in liquid steel increased dramatically with increasing Al content (Figure 7a,b). When the CaO/Al_2O_3 ratio was fixed at 1.5, and the Al content remained the same, the Mg content increased slightly with increasing basicity, and the increasing trend was enhanced when the Al content increased (Figure 7a). When the basicity (B) was fixed at 6, the Mg content was clearly affected by the CaO/Al_2O_3 ratio; a higher CaO/Al_2O_3 ratio in slag corresponded to a higher Mg content in liquid steel (Figure 7b). This suggests that the effect of slag on liquid steel became stronger as the basicity and CaO/Al_2O_3 ratio increased.

In industrial production, the CaO/Al_2O_3 ratio of the refining slag was 1.49, the content of acid-soluble aluminum was 0.024 wt%, and the basicity was 6.12. Based on the IMCT, the calculated equilibrium Mg was about 0.82 ppm, which was lower than the measured value 1.4 ppm. It is because that the effect of the lining has not been taken into account, and this will be discussed in the next section.

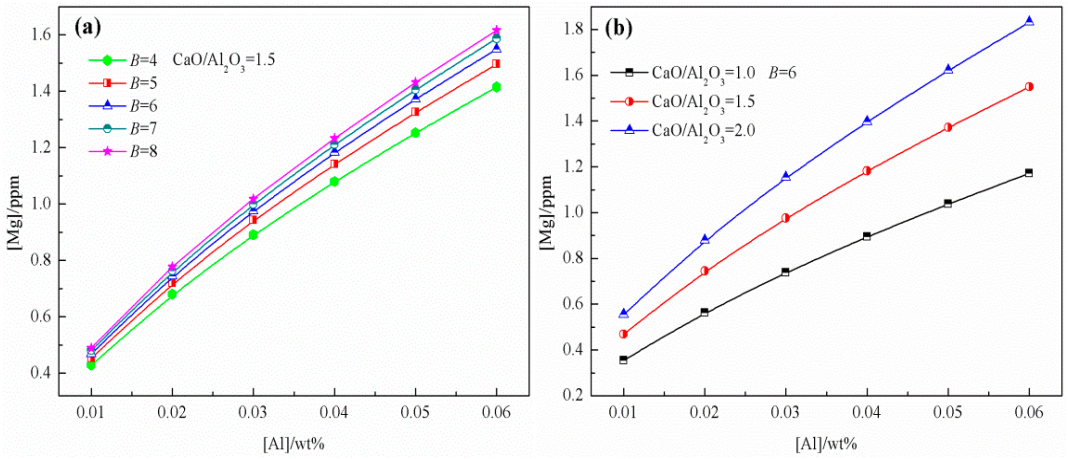

Figure 7. Al–Mg equilibria at various basicities and CaO/Al_2O_3ratiosin the slag: (**a**) Effect of basicities at a fixed CaO/Al_2O_3 ratio; (**b**) effect of CaO/Al_2O_3 ratios at a fixed basicity.

3.2. Effect of Lining on the Mg Content in Liquid Steel

Currently, MgO is a common component in refractory materials. When the bulk steel has a high Al content, the MgO in the lining can be reduced, and can further lead to the generation of $MgO{\cdot}Al_2O_3$ spinel inclusions. For the refractory, $N_{MgO} = 1$. According to Equation (17), the following thermodynamic model of MgO in the refractory reduced by Al can be obtained at $T = 1853$ K:

$$[\%Mg] = 1.44 \times 10^{-3.17} \left(\frac{[\%Al]^2}{N_{Al_2O_3}}\right)^{\frac{1}{3}}. \quad (18)$$

Based on Equation (18), the relationship between Mg and Al content was obtained (Figure 8). The influence of liquid steel on the refractory increases with an increasing content of Al, which leads to the supply of Mg, and the increasing trend is closely related to the slag compositions, especially the CaO/Al_2O_3 ratio, as shown in Figure 8b. For a fixed Al content, the Mg content is higher when the effect of the slag is considered compared to when this effect is ignored. This is attributed to the fact that the slag can absorb Al_2O_3 inclusions, and its ability to absorb inclusions increases with increasing basicity, resulting in an increased Mg content (Figure 8a).

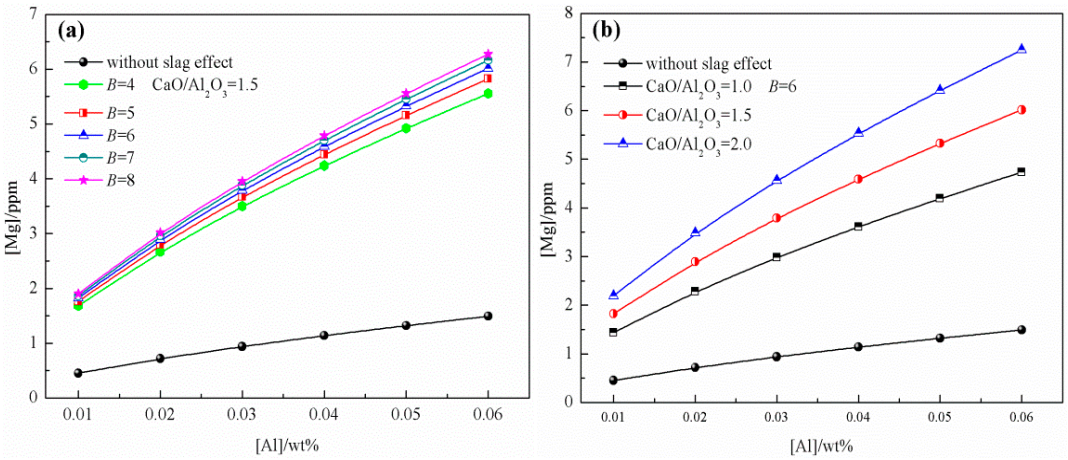

Figure 8. Al–Mg equilibria at various basicities and CaO/Al_2O_3 ratios in the lining: (**a**) Effect of basicities at a fixed CaO/Al_2O_3 ratio; (**b**) effect of CaO/Al_2O_3 ratios at a fixed basicity.

According to the calculation result based on the IMCT, in industrial production, the equilibrium Mg content was 3.2 ppm. Although the real balance is not reached, it indicated that the MgO-based

refractory has a greater potential to supply more Mg into liquid steel than refining slag, which has been verified by Liu [31]. Due to the simultaneous effect of slag and refractory, the Mg content in bulk steel has the enough chance to reach 1.4 ppm. Based on the reported phase stability diagram of Al_2O_3, $MgO{\cdot}Al_2O_3$, and MgO [16,17,24,67], and calculated stability diagram of Mg–Al–O system in liquid steel [13,68], the [Mg%] and [Al%] mainly existed in the spinel generation zone, which is the dominating reason for the generation of $MgO{\cdot}Al_2O_3$ inclusions. It shows a good agreement with the fact that No $MgO{\cdot}Al_2O_3$ spinel inclusions were found before LF, and the $MgO{\cdot}Al_2O_3$ inclusions began to occur during LF process (Figure 5). In order to verify the model at real equilibrium conditions, the laboratory experiment will be carried out in the future work.

3.3. Effect of C on the Mg Content Under RH Conditions

The reduction of MgO by C under RH conditions can be written as the following [69]:

$$(\mathrm{MgO}) + [\mathrm{C}] = [\mathrm{Mg}] + \mathrm{CO}_{(g)}, \Delta G^0 = 722976.29 - 281.59T\ (\frac{\mathrm{J}}{\mathrm{mol}}), \tag{19}$$

with

$$K = \frac{P_{\mathrm{CO}}{\cdot}a_{\mathrm{Mg}}}{a_{\mathrm{MgO}}{\cdot}a_{\mathrm{C}}} = \frac{f_{\mathrm{Mg}}{\cdot}[\%\mathrm{Mg}]{\cdot}P_{\mathrm{CO}}}{f_{\mathrm{C}}{\cdot}[\%\mathrm{C}]{\cdot}N_{\mathrm{MgO}}}. \tag{20}$$

Substituting f_{C} = 1.107, f_{Mg} = 0.781, and [%C] = 0.51 into Equation (20) gives the following formula for slag at 1853 K:

$$[\%\mathrm{Mg}] = 0.72 \times 10^{-5.67} \frac{N_{\mathrm{MgO}}}{P_{\mathrm{CO}}}. \tag{21}$$

For the refractory, N_{MgO} = 1, which gives,

$$[\%\mathrm{Mg}] = 0.72 \times 10^{-5.67} \frac{1}{P_{\mathrm{CO}}} \tag{22}$$

where P_{CO} is the pressure of CO. Equations (21) and (22) represent the theoretical models for the reduction of MgO by C under RH conditions. Based on the IMCT, the effect of C on Mg content under RH conditions at different P_{CO} values was obtained. The content of Mg increases dramatically with decreasing P_{CO}, when C reduces the MgO in slag or lining, and the reduction of MgO in the lining is more crucial. When $\log(P_{\mathrm{CO}}/\mathrm{Pa})$ reached 3.7 (i.e., $P_{\mathrm{CO}} \approx 5066.25$ Pa), [%Mg] was about 0. Therefore, when the CO pressure was sufficiently high, the reduction of MgO in the slag or lining was insignificant. Figure 9 shows the effects of basicity and the CaO/Al_2O_3 ratio in the slag on the Mg content. For a fixed CO pressure, the effect of basicity and the CaO/Al_2O_3 ratio on Mg resulting from the reduction of MgO by C in the slag can be ignored.

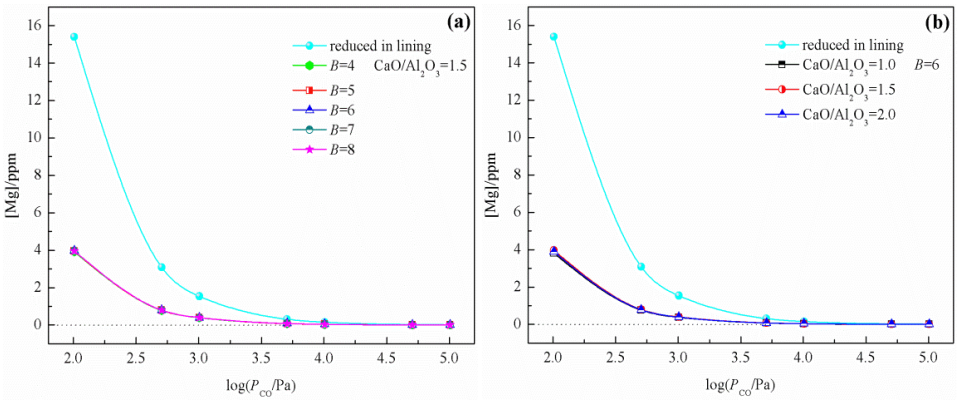

Figure 9. Effects of C on Mg content under RH conditions at different P_{CO}: (**a**) Effect of basicities at a fixed CaO/Al_2O_3 ratio; (**b**) effect of CaO/Al_2O_3 ratios at a fixed basicity.

In actual production, the P_{CO} was about 67 Pa. In this case, the Mg content balanced with lining and slag can reach up to 17 ppm and 5 ppm, respectively, based on the IMCT. Therefore, the supply of Mg into bulk steel under RH conditions is more crucial. In this study, the number of $MgO{\cdot}Al_2O_3$ spinel inclusions and the mass fraction of MgO in $MgO{\cdot}Al_2O_3$ spinel inclusions (Figure 5) increased after RH. These were attributed to the fact that, under RH conditions, the MgO in the slag or lining was partly reduced by C to generate $MgO{\cdot}Al_2O_3$ inclusions; on the other hand, the excess Mg can also combine with $MgO{\cdot}Al_2O_3$ to increase the mass fraction of MgO in $MgO{\cdot}Al_2O_3$ inclusions. The trend of the model calculation is in agreement with the industrial test results. After Ca treatment, some of the inclusions were not modified and existed as independent spherical $MgO{\cdot}Al_2O_3$ inclusions, while others were partly modified (Figure 3). To inhibit the formation of undesirable $MgO{\cdot}Al_2O_3$ spinel inclusions, the pressure of CO could be adjusted to decrease inclusion generation. Furthermore, the appropriate application of Ca treatment can ensure that $MgO{\cdot}Al_2O_3$ spinel inclusions are completely modified into liquid $MgO–Al_2O_3–CaO$-type inclusions.

4. Conclusions

The causes of nozzle clogging during casting and the existent forms of $MgO{\cdot}Al_2O_3$ spinel inclusions in the steel billet were investigated. Based on the IMCT, the MAC model of $CaO–SiO_2–Al_2O_3–MgO–FeO–MnO$ slag was developed, and the generation mechanism of $MgO{\cdot}Al_2O_3$ inclusions, along with the influential factors, were clarified. The conclusions of the present study are as follows:

1. The XRD and SEM/EDS analyses indicated that the nozzle clogging for 51CrV4 spring steel production was primarily due to the presence of $MgAl_2O_4$ spinel inclusions;
2. Three types of $MgO{\cdot}Al_2O_3$ spinel inclusions were observed in steel billets by non-aqueous electrolysis: Pure $MgO{\cdot}Al_2O_3$ inclusions; modified $MgO{\cdot}Al_2O_3$ spinel inclusions containing Mg, Al, Ca, and O, which was the dominant inclusion type; and modified spinel inclusions primarily containing Al, Ca, and O. The assessment of the inclusions in the specimens before and after LF and RH indicated that the inclusions transformed through $Al_2O_3 \rightarrow MgO{\cdot}Al_2O_3 \rightarrow MgO–Al_2O_3–CaO$ during the refining process;
3. The generation mechanism of $MgO{\cdot}Al_2O_3$ inclusions in 51CrV4 spring steel refined by $CaO–SiO_2–Al_2O_3–MgO–FeO–MnO$ slag was evaluated based on the IMCT combined with industrial results. The effects of slag composition, refractory, and RH conditions on the content of Mg in liquid steel were determined. Model calculation results indicated that the Mg content increased with an increasing basicity, CaO/Al_2O_3 ratio, and Al content during LF, with the CaO/Al_2O_3 ratio being the most critical factor. In contrast, under RH conditions, the effects of basicity and the CaO/Al_2O_3 ratio were insignificant, and the partial pressure of CO was the dominant factor.

Author Contributions: Methodology, D.Z. and J.L.; formal analysis, H.Z.; investigation, Z.X.; writing—review and editing, J.L.

Funding: This research was funded by the National Natural Science Foundation of China (Grant No. 51704105, No. 51874214, No. 51604198).

Acknowledgments: The authors would like to thank the National Natural Science Foundation of China (Grant No. 51704105, No. 51874214, No. 51604198). The resources were partially provided by the State Key Laboratory of Refractories and Metallurgy, Wuhan University of Science and Technology.

Conflicts of Interest: The authors declare no conflicts of interest.

References

1. Yao, D.; Li, J.; Li, J.; Zhu, Q. Effect of cold rolling on morphology of carbides and properties of 7Cr17MoV stainless steel. *Mater. Manuf. Process.* **2015**, *30*, 111–115. [CrossRef]
2. Park, J.H.; Todoroki, H. Control of $MgO{\cdot}Al_2O_3$ spinel inclusions in stainless steels. *ISIJ Int.* **2010**, *50*, 1333–1346. [CrossRef]

3. Fukaura, K.; Yokoyama, Y.; Yokoi, D.; Tsujii, N. Fatigue of cold-work tool steels: Effect of heat treatment and carbide morphology on fatigue crack formation, life, and fracture surface observations. *Metall. Mater. Trans. A* **2004**, *35*, 1289–1300. [CrossRef]
4. Atkinson, H.V.; Shi, G. Characterization of inclusions in clean steels: A review including the statistics of extremes methods. *Prog. Mater. Sci.* **2003**, *48*, 457–520. [CrossRef]
5. Wang, Z.; Liu, X.; Xie, F.; Lai, C.; Li, H.; Zhang, Q. Dynamic recrystallization behavior and critical strain of 51CrV4 high-strength spring steel during hot deformation. *JOM* **2018**, *70*, 2385–2391. [CrossRef]
6. Zhang, L.; Gong, D.H.; Li, Y.C.; Wang, X.J.; Ren, X.X.; Wang, E.G. Effect of quenching conditions on the microstructure and mechanical properties of 51CrV4 spring steel. *Metals* **2018**, *8*, 1056. [CrossRef]
7. Hasegawa, M.; Maruhashi, S. Synthetic slag refining of 18Cr steel in VOD. *Tetsu-to-Hagane* **1977**, *63*, 2087–2093. [CrossRef]
8. Nishi, T.; Shinme, K. Formation of spinel inclusions in molten stainless steel under Al deoxidation with slags. *Tetsu-to-Hagane* **1998**, *84*, 837–843. [CrossRef]
9. Jiang, M.; Wang, X.; Chen, B.; Wang, W. Laboratory study on evolution mechanisms of non-metallic inclusions in high strength alloyed steel refined by high basicity slag. *ISIJ Int.* **2010**, *50*, 95–104. [CrossRef]
10. Ganesh, I. A review on magnesium aluminate ($MgAl_2O_4$) spinel: Synthesis, processing and applications. *Cheminform* **2013**, *58*, 63–112. [CrossRef]
11. Sakata, K.; Co, A.S. Technology for production of austenite type clean stainless. *ISIJ Int.* **2006**, *46*, 1795–1799. [CrossRef]
12. Beskow, K.; Tripathi, N.N.; Nzotta, M.; Sandberg, A.; Sichen, D. Impact of slag-refractory lining reactions on the formation of inclusions in steel. *Ironmak. Steelmak.* **2004**, *31*, 514–518. [CrossRef]
13. Yang, S.; Wang, Q.; Zhang, L.; Li, J.; Peaslee, K. Formation and modification of $MgO{\cdot}Al_2O_3$-based inclusions in alloy steels. *Metall. Mater. Trans. B* **2012**, *43*, 731–750. [CrossRef]
14. Yang, W.; Zhang, L.; Wang, X.; Ren, Y.; Liu, X.; Shan, Q. Characteristics of inclusions in low carbon Al-killed steel during ladle furnace refining and calcium treatment. *ISIJ Int.* **2013**, *53*, 1401–1410. [CrossRef]
15. Itoh, H.; Hino, M.; Ban-Ya, S. Thermodynamics on the formation of spinel nonmetallic inclusion in liquid steel. *Metall. Mater. Trans. B* **1997**, *28*, 953–956. [CrossRef]
16. Jiang, M.; Wang, X.; Chen, B.; Wang, W. Formation of $MgO{\cdot}Al_2O_3$ inclusions in high strength alloyed structural steel refined by CaO–SiO_2–Al_2O_3–MgO slag. *ISIJ Int.* **2008**, *48*, 885–890. [CrossRef]
17. Jiang, M.; Wang, X.H.; Wang, W.J. Control of non-metallic inclusions by slag-metal reactions for high strength alloying steels. *Steel Res. Int.* **2010**, *81*, 759–765. [CrossRef]
18. Liu, C.; Huang, F.; Suo, J.; Wang, X. Effect of magnesia-carbon refractory on the kinetics of $MgO{\cdot}Al_2O_3$ spinel inclusion generation in extra-low oxygen steels. *Metall. Mater. Trans. B* **2016**, *47*, 989–998. [CrossRef]
19. Giordani, E.J.; Guimara, V.A.; Pinto, T.B.; Ferreira, I. Effect of precipitates on the corrosion-fatigue crack initiation of ISO 5832-9 stainless steel biomaterial. *Int. J. Fatigue* **2004**, *26*, 1129–1136. [CrossRef]
20. Yin, X.; Sun, Y.H.; Yang, Y.D.; Bai, X.F.; Deng, X.X.; Barati, M.; McLean, A. Inclusion evolution during refining and continuous casting of 316L stainless steel. *Ironmak. Steelmak.* **2016**, *43*, 533–540. [CrossRef]
21. Park, J.H.; Kim, D.S. Effect of CaO–Al_2O_3–MgO slags on the formation of MgO–Al_2O_3 inclusions in ferritic stainless steel. *Metall. Mater. Trans. B Process Metall. Mater. Process. Sci.* **2005**, *36*, 495–502. [CrossRef]
22. Todoroki, H.; Mizuno, K.; Noda, M.; Tohge, T. Formation mechanism of spinel type inclusion in 304 stainless steel deoxidized with ferosilicon alloys. In *Proceedings of the 84th Steelmaking Conference*; ISS: Warrendale, PA, USA, 2001; Volume 331.
23. Todoroki, H.; Mizuno, K. Effect of silica in slag on inclusion compositions in 304 stainless steel deoxidized with aluminum. *ISIJ Int.* **2004**, *44*, 1350–1357. [CrossRef]
24. Kawakami, K.; Taniguchi, T.; Nakashima, K. Generation mechanisms of non-metallic inclusions in high-cleanliness steel. *Tetsu-to-Hagane* **2007**, *93*, 743–752. [CrossRef]
25. Brabie, V. Mechanism of reaction between refractory materials and aluminum deoxidised molten steel. *ISIJ Int.* **1996**, *36*, 109–112. [CrossRef]
26. Okuyama, G.; Yamaguchi, K.; Takeuchi, S.; Sorimachi, K. Effect of slag composition on the kinetics of formation of Al_2O_3-MgO inclusions in aluminum killed ferritic stainless steel. *ISIJ Int.* **2000**, *40*, 121–128. [CrossRef]
27. Shin, J.H.; Park, J.H. Effect of CaO/Al_2O_3 ratio of ladle slag on formation behavior of inclusions in Mn and V alloyed steel. *ISIJ Int.* **2018**, *58*, 88–97. [CrossRef]

28. Chen, G.; Guo, Y.; He, S. Effect of FeO content in slag on formation of $MgO{\cdot}Al_2O_3$ inclusion for Al-killed steel. *Metall. Res. Technol.* **2016**, *113*, 204–213. [CrossRef]
29. Suito, H.; Inoue, R. Thermodynamics on control of inclusions composition in ultra-clean steels. *ISIJ Int.* **1996**, *36*, 528–536. [CrossRef]
30. Shin, J.H.; Chung, Y.; Park, J.H. Refractory–slag–metal–inclusion multiphase reactions modeling using computational thermodynamics: Kinetic model for prediction of inclusion evolution in molten steel. *Metall. Mater. Trans. B* **2017**, *48*, 46–59. [CrossRef]
31. Liu, C.; Huang, F.; Wang, X. The effect of refining slag and refractory on inclusion transformation in extra low oxygen steels. *Metall. Mater. Trans. B* **2016**, *47*, 999–1009. [CrossRef]
32. Brabie, V. A study on the mechanism of reaction between refractory materials and aluminium deoxidised molten steel. *Steel Res.* **1997**, *68*, 54–60. [CrossRef]
33. Liu, C.; Yagi, M.; Gao, X.; Kim, S.J.; Huang, F.; Ueda, S.; Kitamura, S.Y. Dissolution behavior of Mg from magnesia-chromite refractory into Al-killed molten steel. *Metall. Mater. Trans. B* **2018**, *49*, 2298–2307. [CrossRef]
34. Alhussein, A.; Yang, W.; Zhang, L.F. Effect of interactions between Fe–Al alloy and MgO-based refractory on the generation of $MgO{\cdot}Al_2O_3$ spinel. *Ironmak. Steelmak.* **2019**, 1–8. [CrossRef]
35. Wang, H.; Glaser, B.; Sichen, D. Improvement of resistance of MgO-based refractory to slag penetration by in situ spinel formation. *Metall. Mater. Trans. B* **2015**, *46*, 749–757. [CrossRef]
36. Huang, F.; Zhang, L.; Zhang, Y.; Ren, Y. Kinetic modeling for the dissolution of MgO lining refractory in Al-killed steels. *Metall. Mater. Trans. B* **2017**, *48*, 2195–2206. [CrossRef]
37. Ren, Y.; Zhang, L.F. Thermodynamic model for prediction of slag-steel-inclusion reactions of 304 stainless steels. *ISIJ Int.* **2017**, *57*, 68–75. [CrossRef]
38. Park, J.H. Thermodynamic investigation on the formation of inclusions containing $MgAl_2O_4$ spinel during 16Cr–14Ni austenitic stainless steel manufacturing processes. *Mater. Sci. Eng. A* **2008**, *472*, 43–51. [CrossRef]
39. Yang, W.; Zhang, L.F.; Duan, H.; Ren, Y.; Wang, J.; Liu, X. Formation of non-metallic inclusions in the molten steel in MgO crucibles. In *EPD Congress 2014*; John Wiley & Sons: Hoboken, NJ, USA, 2014; pp. 269–276.
40. Jansson, S.; Brabie, V.; Jönsson, P. Magnesia–carbon refractory dissolution in Al killed low carbon steel. *Ironmak. Steelmak.* **2006**, *33*, 389–397. [CrossRef]
41. Duan, S.C.; Guo, X.L.; Guo, H.J.; Guo, J. A manganese distribution prediction model for $CaO–SiO_2–FeO–MgO–MnO–Al_2O_3$ slags based on IMCT. *Ironmak. Steelmak.* **2017**, *44*, 168–184. [CrossRef]
42. Duan, S.C.; Li, C.; Guo, X.L.; Guo, H.J.; Guo, J.; Yang, W.S. A thermodynamic model for calculating manganese distribution ratio between $CaO–SiO_2–MgO–FeO–MnO–Al_2O_3–TiO_2–CaF_2$ ironmaking slags and carbon saturated hot metal based on the IMCT. *Ironmak. Steelmak.* **2017**, *45*, 655–664. [CrossRef]
43. Li, B.; Li, L.; Guo, H.; Guo, J.; Duan, S.; Sun, W. A phosphorus distribution prediction model for CaO–SiO2–MgO–FeO–Fe2O3–Al2O3–P2O5 slags based on the IMCT. *Ironmak. Steelmak.* **2019**, 1–10. [CrossRef]
44. Yang, X.M.; Li, J.Y.; Chai, G.M.; Duan, D.P.; Zhang, J. A Thermodynamic model for predicting phosphorus partition between CaO-based slags and hot metal during hot metal dephosphorization pretreatment process based on the ion and molecule coexistence theory. *Metall. Mater. Trans. B* **2016**, *47*, 2279–2301. [CrossRef]
45. Yang, X.M.; Duan, J.P.; Shi, C.B.; Zhang, M.; Zhang, Y.L.; Wang, J.C. A thermodynamic model of phosphorus distribution ratio between $CaO–SiO_2–MgO–FeO–Fe_2O_3–MnO–Al_2O_3–P_2O_5$ slags and molten steel during a top-bottom combined blown converter steelmaking process based on the ion and molecule coexistence theory. *Metall. Mater. Trans. B* **2011**, *42*, 738–770. [CrossRef]
46. Yang, X.M.; Shi, C.B.; Zhang, M.; Duan, J.P.; Zhang, J. A thermodynamic model of phosphate capacity for $CaO–SiO_2–MgO–FeO–Fe_2O_3–MnO–Al_2O_3–P_2O_5$ slags equilibrated with molten steel during a top-bottom combined blown converter steelmaking process based on the ion and molecule coexistence theory. *Metall. Mater. Trans. B* **2011**, *42*, 951–977. [CrossRef]
47. Yang, X.M.; Zhang, M.; Chai, G.M.; Li, J.Y.; Liang, Q.; Zhang, J. Thermodynamic models for predicting dephosphorisation ability and potential of $CaO–FeO–Fe_2O_3–Al_2O_3–P_2O_5$ slags during secondary refining process of molten steel based on ion and molecule coexistence theory. *Ironmak. Steelmak.* **2016**, *43*, 663–687. [CrossRef]
48. Li, J.Y.; Zhang, M.; Guo, M.; Yang, X.M. Enrichment mechanism of phosphate in $CaO–SiO_2–FeO–Fe_2O_3–P_2O_5$ steelmaking slags. *Metall. Mater. Trans. B* **2014**, *45*, 1666–1682. [CrossRef]

49. Yang, X.M.; Li, J.Y.; Zhang, M.; Yan, F.J.; Duan, D.P.; Zhang, J. A further evaluation of the coupling relationship between dephosphorization and desulfurization abilities or potentials for CaO-based slags: Influence of slag chemical composition. *Metals* **2018**, *8*, 1083. [CrossRef]
50. Shi, C.B.; Yang, X.M.; Jiao, J.S.; Li, C.; Guo, H.J. A sulphide capacity prediction model of $CaO–SiO_2–MgO–Al_2O_3$ ironmaking slags based on the ion and molecule coexistence theory. *ISIJ Int.* **2010**, *50*, 1362–1372. [CrossRef]
51. Yang, X.M.; Shi, C.B.; Zhang, M.; Chai, G.M.; Wang, F. A thermodynamic model of sulfur distribution ratio between $CaO–SiO_2–MgO–FeO–MnO–Al_2O_3$ slags and molten steel during LF refining process based on the ion and molecule coexistence theory. *Metall. Mater. Trans. B* **2011**, *42*, 1150–1180. [CrossRef]
52. Yang, X.M.; Zhang, M.; Shi, C.B.; Chai, G.M.; Zhang, J. A sulfide capacity prediction model of $CaO–SiO_2–MgO–FeO–MnO–Al_2O_3$ slags during the LF refining process based on the ion and molecule coexistence theory. *Metall. Mater. Trans. B* **2012**, *43*, 241–266. [CrossRef]
53. Yang, X.M.; Li, J.Y.; Zhang, M.; Chai, G.M.; Zhang, J. Prediction model of sulfide capacity for $CaO–FeO–Fe_2O_3–Al_2O_3–P_2O_5$ slags in a large variation range of oxygen potential based on the ion and molecule coexistence theory. *Metall. Mater. Trans. B* **2014**, *45*, 2118–2137. [CrossRef]
54. Yang, X.M.; Li, J.Y.; Zhang, M.; Zhang, J. Prediction model of sulphur distribution ratio between $CaO–FeO–Fe_2O_3–Al_2O_3–P_2O_5$ slags and liquid iron over large variation range of oxygen potential during secondary refining process of molten steel based on ion and molecule coexistence theory. *Ironmak. Steelmak.* **2016**, *43*, 39–55. [CrossRef]
55. Yang, X.M.; Zhang, M.; Zhang, J.L.; Li, P.C.; Li, J.Y.; Zhang, J. Representation of oxidation ability for metallurgical slags based on the ion and molecule coexistence theory. *Steel Res. Int.* **2014**, *85*, 347–375. [CrossRef]
56. Zhang, J. *Computational Thermodynamics of Metallurgical Melts and Solutions*; Metallurgical Industry Press: Beijing, China, 2007.
57. Verein Deutscher Eisenhuttenleute. *Slag Atlas*, 2nd ed.; Woodhead Publishing Limited: Cambridge, UK, 1995.
58. Chen, J.X. *Common Charts and Databook for Steelmaking*, 2nd ed.; Metallurgical Industry Press: Beijing, China, 2010.
59. Rein, R.H.; Chipman, J. Activities in the liquid solution $SiO_2–CaO–MgO–Al_2O_3$ at 1600 °C. *Trans. Met. Soc. AIME* **1965**, *233*, 415–425.
60. Turkdogan, E.T. *Physical Chemistry of High Temperature Technology*; Academic Press: New York, NY, USA, 1980; pp. 8–12.
61. Gaye, H.; Welfringer, J. *Proceedings of the Second International Symposium on Metallurgical Slags and Fluxes*; Fine, H.A., Gaskell, D.R., Eds.; TMS–AIME: Lake Tahoe, NV, USA, 1984; pp. 357–375.
62. Ban-ya, S.; Chiba, A.; Hikosaka, A. Thermodynamics of $Fe_tO–M_xO_y$ (M_xO_y = CaO, SiO_2, TiO_2, and Al_2O_3) binary melts in equilibrium with solid iron. *Tetsu-to-Hagane* **1980**, *66*, 1484–1493. [CrossRef]
63. Timucin, M.; Muan, A. Activity–composition relations in $NiAl_2O_4–MnAl_2O_4$ solid solutions and stabilities of $NiAl_2O_4$ and $MnAl_2O_4$ at 1300 °C and 1400 °C. *J. Am. Ceram. Soc.* **1992**, *75*, 1399–1406. [CrossRef]
64. Barin, I.; Knacke, O.; Kubaschewski, O. *Thermochemical Properties of Inorganic Substances (Supplement)*; Springer: New York, NY, USA, 1977; pp. 392–445.
65. Itoh, H.; Hino, M.; Ban-ya, S. Deoxidation equilibrium of magnesium in liquid iron. *Tetsu-to-Hagane* **1997**, *83*, 623–628. [CrossRef]
66. Huang, X.H. *Theory of Iron and Steel Metallurgy*, 3rd ed.; Metallurgical Industry Press: Beijing, China, 2002.
67. Sun, Y.H.; Zeng, Y.N.; Xu, R.; Cai, K.K. Formation mechanism and control of $MgO·Al_2O_3$ inclusions in non-oriented silicon steel. *Int. J. Min. Met. Mater.* **2014**, *21*, 1068–1076. [CrossRef]
68. Ren, Y.; Zhang, L.F.; Fang, W. Effect of addition of Al-based slag deoxidizer on $MgO·Al_2O_3$ inclusions in 3Si-Fe steels. *Metall. Res. Technol.* **2016**, *114*, 108–116. [CrossRef]
69. Tang, H.Y.; Wu, T.; Wang, J.L.; Liang, Y.C.; Li, J. Mass action concentration model of $CaO–MgO–FeO–Al_2O_3–SiO_2$ slag systems and its application to the formation mechanism of $MgO·Al_2O_3$ spinel-type inclusion in casing steel. *Metall. Res. Technol.* **2015**, *112*, 409–423. [CrossRef]